Materials Science & Engineering A 755 (2019) 211–219

Contents lists available at ScienceDirect

Materials Science & Engineering A

journal homepage: www.elsevier.com/locate/msea

Effect of zirconium on the properties of polycrystalline Cu-Al-Be shape memory alloy

Guniputi Bala Narasimha, S.M. Murigendrappa*

Department of Mechanical Engineering, National Institute of Technology Karnataka, Surathkal, 575025, India

ARTICLE INFO

Keywords:
Cu–Al-Be shape memory alloy
Zirconium
Grain refinement
Precipitation strengthening
Hydrogen embrittlement

ABSTRACT

This paper presents an investigation of the effect of zirconium on the properties of polycrystalline Cu-Al-Be shape memory alloy. Mechanical and shape memory properties have been evaluated by varying the compositions of Zr to $Cu_{88.13}$-$Al_{11.42}$-$Be_{0.45}$ alloy ranging from 0.05 to 0.4 wt% with step 0.1 wt%. The results unveil reduction in the grain size of 89.18% with the improved tensile strength of 667 ± 30 MPa and ductility of 23.95 ± 0.86% and excellent shape recovery ratio of 100% with the addition of Zr up to 0.3 wt%. Increase in transformation temperatures is observed with the addition of Zr.

1. Introduction

Past two decades, smart materials draw huge attention among the researchers towards development and application in the fields of aviation [1], civil structures [2], biomedical and automation industries [3]. Shape memory alloys (SMA), Shape memory polymers (SMP), Hydrogels, Electrostrictive (ES), Piezoelectric (PE), and Magnetostrictive (MS) are the most common smart materials [4]. Among these, shape memory alloys holds a peculiar property viz. deformed material can restore their actual shape either by an increase in temperature or removal of the load, known as shape memory effect and super-elasticity [5] respectively. These two distinct properties attract the usage of SMA's as actuators in smart structures [6] and civil structures to isolate and suppress vibration. Cu-Al based shape memory alloys are chosen as an alternative to Ni-Ti (Nitinol), because of ease of production [7] and economical [8]. However, the applications are narrowed to real-time because of intergranular fracture [9], rapid deterioration of shape memory due to phase stabilization [10] and dislocations [11]. The major limitation related to copper-based shape memory alloys is intergranular fracture attributed to coarse grain size [12–14].

The Intergranular fracture can be suppressed by refinement of grain size, in turn, to increase the ductility and mechanical strength. Many researchers have investigated on grain refinement by adopting various techniques, i.e., addition of grain refiners [15–18], rapid solidification [19–21], severe plastic deformation [12,22], and thermal treatments [23,24] to enhance the properties of alloys. Rapid solidification and severe plastic deformation techniques are highly impractical for bulk alloys [25]. Addition of grain refiners/inoculants is a simple and efficient technique for the refinement of bulk alloys compared to the above techniques. Based on existing literature, zirconium played a significant role in grain refinement and are presented here. Gil et al. [26] studied the effect of Co, Mn, Si and Zr grain refiners on kinetic growth of grains in Cu-Zn-Al alloys, subjected to different isothermic treatments. They observed that the growth exponent of Zr doped alloy is very low compared to other refiners. Matsuoka et al. [27] and Lee et al. [28] examined the addition of Zr and Ti to Cu-Al-Ni alloys, discerned fine grain refinement and improved ductility with Zr compared to Ti and increase in Ms temperatures with the increase in Zr content. Lee et al. [29] probed the effect of B, Cr, Ti, V and Zr on Cu-Zn-Al alloys, and found the maximum reduction in grain size for Zr doped alloys, without any modification in the shape memory effect. The influence of Zr doped Cu-A1-Ni alloy have been reported by Kim et al. [30,31], and the results unveil that refined grain with a significant increase in fracture strength and fracture strain. They also observed that the maximum shape recovery of 95% occurred at 3% strain, and decreases with an increase in the percentage of strains. Bhattacharya et al. [32] observed significant grain refinement with doping of Zr. Hsu et al. [33] investigated superplastic forming behavior on Cu-Zn-Al alloy with Zr and observed that the grain size decreases as annealing temperature lowers. Sampath et al. investigated the effect of Zr on Cu-Al-Ni [34], Cu-Zn-Al [35] and Cu-Al-Mn [36] alloys, noticed a significant improvement in grain refinement, ductility, and hardness with increase in wt.% of Zr, except in Cu-Al-Mn alloys. Shape recovery studies of the Zr doped alloys exhibit an increase in the percentages of shape recovery for Cu-Zn-Al, whereas it decreases in Cu-Al-Mn alloys, attributes to the relation between size and width of martensite variants and its

* Corresponding author.
E-mail addresses: balanarasimha.g@gmail.com (G. Bala Narasimha), smm@nitk.ac.in (S.M. Murigendrappa).

https://doi.org/10.1016/j.msea.2019.04.022
Received 28 November 2018; Received in revised form 26 February 2019; Accepted 5 April 2019
Available online 06 April 2019
0921-5093/

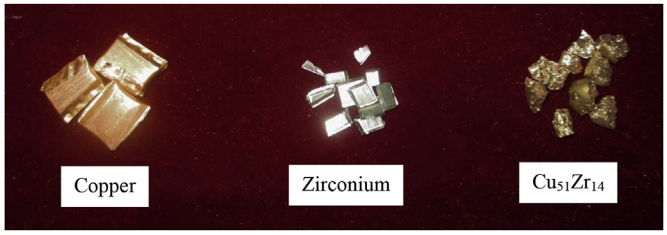

Fig. 1. Photograph of copper, zirconium and $Cu_{51}Zr_{14}$ master alloy.

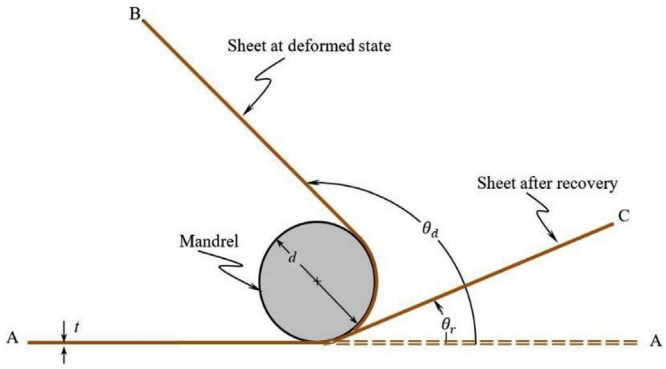

Fig. 2. Schematic of bend test for shape recovery ratio.

reorientation. Yang et al. [37] examined the effect CuZr inoculant on Cu-Al-Mn alloy and discerned improved properties with the doping of inoculant.

It is assimilated from the literature that, the rate of growth of grains lags in Zr doped alloys compared to other grain refiners, results in grain refinement and improved mechanical properties. In inference, no work has been reported on the effect of Zr doped Cu-Al-Be alloy, and this drives us to investigate its effect in enhancing the properties of alloys.

2. Experimental

2.1. Alloy and specimen preparation

Cu-Al-Be alloy with the nominal composition of Cu $_{88.13}$ – Al $_{11.42}$ – Be $_{0.45}$ (wt. %), doped with minor amounts of Zr varies from 0.05 – 0.4 wt % to the base alloys were prepared using raw materials of purity > 99.9%. At first, CuZr master alloy with the atomic ratio of 51:14 was prepared using vacuum arc remelting machine (Make: Edmund Buhler GmbH, Model: AM/0.5) in the form of small buttons and sheared into small pieces as shown in Fig. 1.

The mixture of Cu, Al and Be metals as per the nominal composition was melted in an induction furnace under argon gas (99.99%) atmosphere, cast and sectioned into six equal parts. Further, the grain refiner Zr was added to the each sectioned part, remelted and cast in the form of a plate of size 150 × 150 × 3 mm. The alloys Cu $_{88.13}$ – Al $_{11.42}$ – Be $_{0.45}$ with 0, 0.05, 0.1, 0.2, 0.3 and 0.4 wt % of Zr are designated with Z_0,

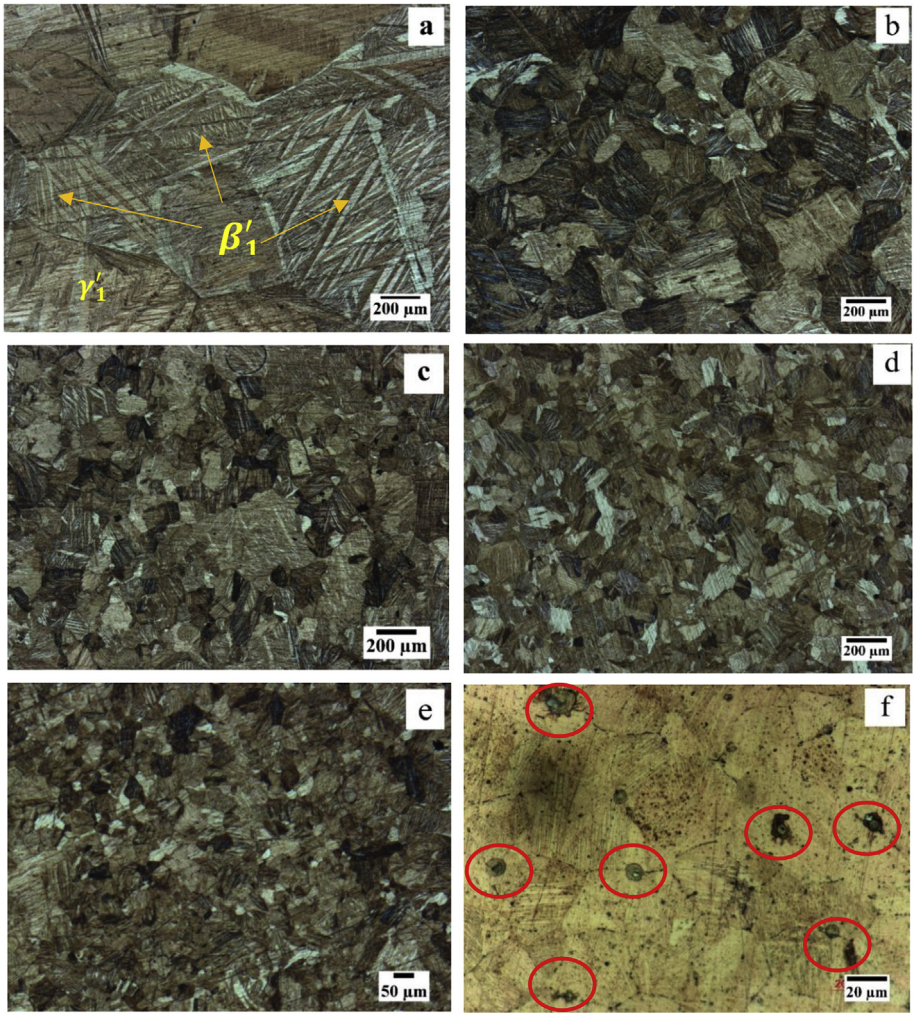

Fig. 3. Microstructures of alloys; (a) Z_0 – 50 × , (b) Z_1 – 50 × , (c) Z_2 – 50 × , (d) Z_3 – 50 × , (e) Z_4 – 50 and (f) Z_5 – 500 × .

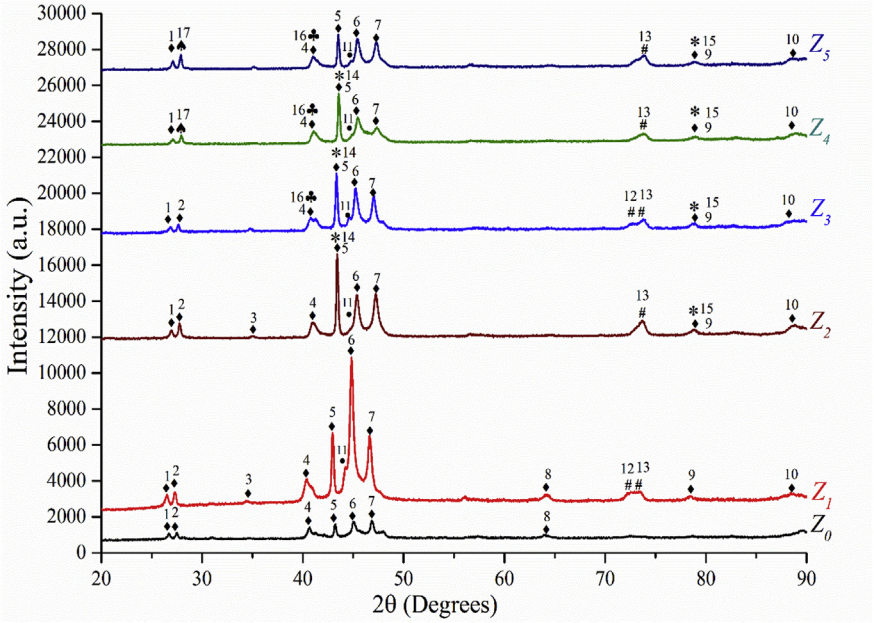

♦ β_1' - 1 (111), 2 (019), 3 (020), 4 (202), 5 (00 22), 6 (12 10), 7 (20 12), 8 (12 20), 9 (12 26), 10 (248)
● γ_1' - 11 (002), # **ZrAl3** - 12 (303), 13 (11 12), ***Cu5Zr** – 14 (311), 15 (440), ♣ **AlCu2Zr** –16 (110)
♠ **Zr02** - 17 (-111)

Fig. 4. X-ray diffractograms of alloys; Z_0, Z_1, Z_2, Z_3, Z_4 and Z_5.

Z_1, Z_2, Z_3, Z_4, and Z_5, respectively. Homogenization of alloys was carried out for 4 h at 800 °C under argon gas atmosphere, followed by forced air cooling to room temperature to avoid quench cracks [38]. Microstructural and tensile specimens were cut from the homogenized alloy plates utilizing wire electric discharge machine. An alloy of 3 mm thickness plate were hot rolled at 800 °C into a sheet of thickness 0.5 mm with intermediate annealing. Rolled sheets were betatized at 850 °C for 15 min and quenched into the water at room temperature for shape recovery studies.

2.2. Characterization

Specimens for the characterization were betatized at 850 °C for 15 min followed by quenching in water at room temperature for 10 min. After quenching, the specimens were ultrafine polished with saturated colloidal alumina suspension and etched with a solution of 2 g of FeCl3, 2 ml of HCl and 95 ml of methanol for microstructure and SEM studies. The Mean grain size of the alloys was obtained by adopting the ASTM E112 - linear intercept method. Morphology, and precipitates and its elemental composition were obtained using scanning electron microscope (SEM, Make: Zeiss, Model: EVO MA18) attached with EDS (EDS Make: Oxford, Model: X-act). Phases exist in the alloy, and its crystal structure was analyzed with CuKα1 monochromatic radiation (λ = 1.54056 A°), 40 kV and 15 mA from 2θ = 20°–90° at a scan rate of 2°/min using x-ray diffractometer (Make: Rigaku, Model: Miniflex 600) at room temperature. Phase transformation temperatures of the quenched alloys were measured using differential scanning calorimeter (DSC, Make: PerkinElmer, Model: 6000) with a scan rate of 2°/min. Stress-strain curves were recorded using a universal testing machine (Make: Shimazdu, Capacity: 100 kN) as per ASTM E8 with 0.05 mm/min rate of loading. Shape recovery ratio (SRR) of the alloys were measured by the bend test as illustrated in Fig. 2. The test procedure is as follows, the sheet at full martensite state (≤Mf) was bent around a mandrel and unloaded viz. from A-A to A-B, this angle measured as θ_d. The deformed sheet was heated above 10 °C of the austenite finish temperature, and it tends to attain the original position with or without residual strain, i.e., A-C or A-A, respectively, this angle measured as θ_r.

The shape recovery ratio computed using Eq. (1).

$$\eta = \frac{\theta_d - \theta_r}{\theta_d} \quad (1)$$

where θ_d - angle after deformation and θ_r - residual angle after recovery.

3. Results and discussion

3.1. Microstructure

Microstructures of the alloys as depicted in Fig. 3, exhibits grains were completely recrystallized and refined with the addition of Zr. It is observed from Fig. 3a, Z_0 (Zr free) has coarse grains of size 463.45 μm, with zig-zag martensite (18R - β_1') in the form of long spears and a small amount of coarse variants (2H - γ_1'). Addition of Zr to Z_1 and Z_2, i.e., 0.05 and 0.1 wt% to the matrix exhibit bimodal grains (irregular in sizes) as shown in Fig. 3b and c have a grain size of 157.07 and 125.97 μm, respectively. The variations in the grain size of the alloys are due to the irregular distribution of refiner in the matrix, because of minimal addition. Increase in Zr to Z_3 and Z_4, i.e., 0.2 and 0.3 wt%, produces equiaxial grains in lateral and longitudinal directions as shown in Fig. 3d and e, with an average size of 116.49 and 50.13 μm, respectively. Increase in Zr to Z_5 again increases the grain size to 159.02 μm. The percentage of reduction in grain sizes were 0, 66.10, 72.81, 74.86, 89.18 and 65.68% for Z_0, Z_1, Z_2, Z_3, Z_4, and Z_5, respectively. It is manifested that the increase in doping of Zr reduces the grain size up to Z_4 as shown in Fig. 3a–e, ascribed to various mechanisms, i.e.

i) very low grain growth exponent of Zr [26],
ii) uniform dispersion of Zr in the matrix acts as nucleant, i.e., Zr is insoluble in the matrix when quenched to room temperature creates heterogeneous nucleation sites [34,37] and enhances the number of grains and
iii) surplus Zr above the solid solubility limit forms fine spherical precipitates in the grains [36] and precipitates at the grain boundaries

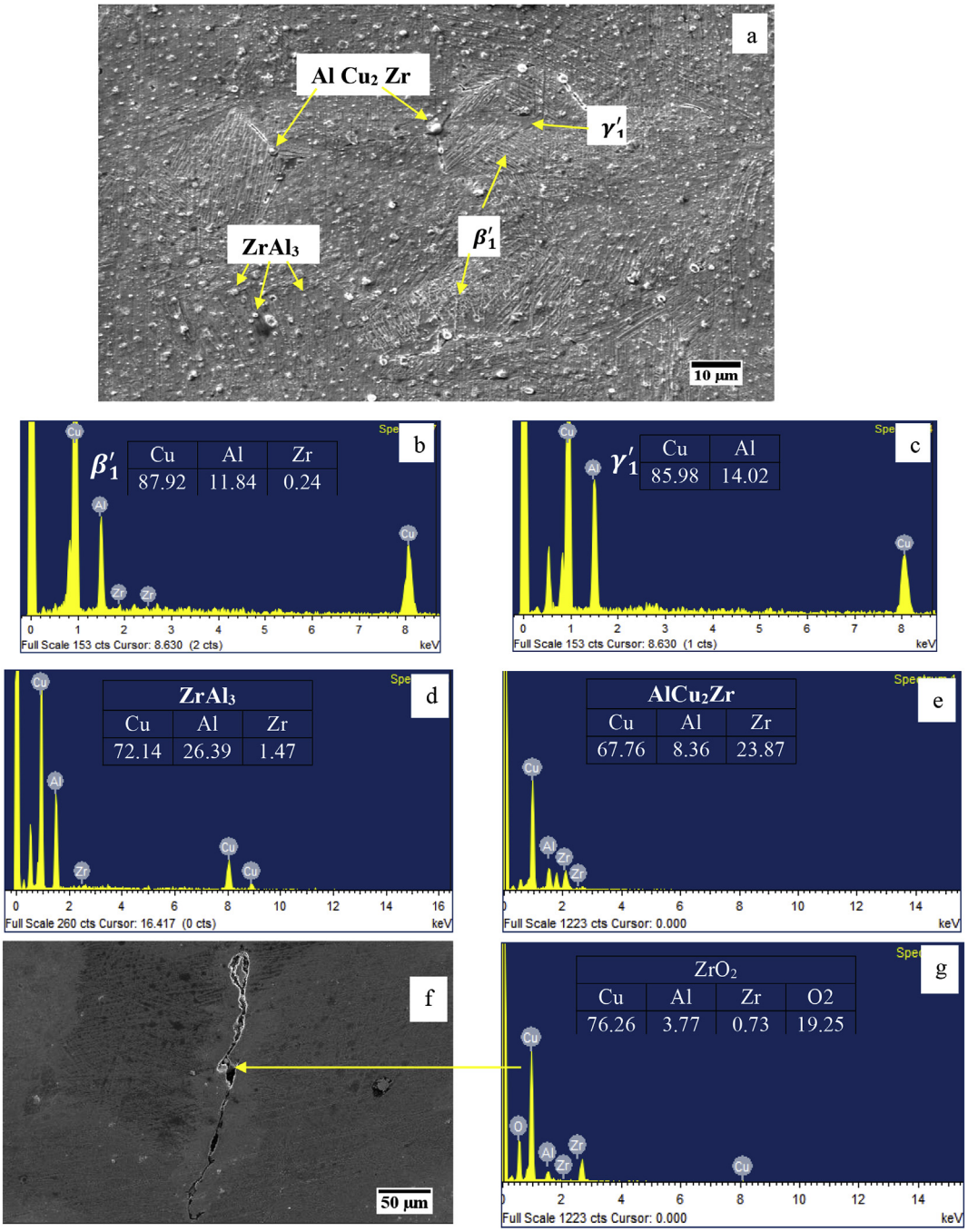

Fig. 5. Secondary electron images - Morphology; (a) Z_4 and (f) Z_5, and EDS; (b) β'_1, (c) γ'_1, (d) $ZrAl_3$, (e) $AlCu_2Zr$ and (g) ZrO_2.

(Fig. 3f) inhibits the grain growth.

It is worth noting that the width and thickness of the martensite plates decrease with the decrease in grain size, with the increase of Zr. The orientation of grains and martensite variants are completely irregular due to rapid quenching from the elevated temperature. Increase in grain size of Z_5 is due to surplus addition of Zr Is highly insoluble in the matrix and agglomerates at the grain boundary as shown in the red colored ellipses of Fig. 3f and also in Fig. 5a causes no refinement.

3.2. Phases and morphology

X-Ray diffractograms depicted in Fig. 4, unveils the phases exists in the alloys. Crystallite size, lattice planes, and parameters were studied from the intensity and width of diffracted peaks. The morphology of the phases with elemental composition presented in the secondary electron images as shown in Fig. 5.

It is discerned from the diffractograms that, Zr-free alloy i.e., Z_0 possess sheer martensite of $\beta_1'(Cu_3Al)$ with little $\gamma_1'(CuAl)$ phase of orthorhombic (18R) and monoclinic (2H) structures, respectively and confirmed from the Fig. 3a. The alloys, Z_1 to Z_5 exhibits the peaks of $ZrAl_3$ corresponds to very fine Al-rich spherical precipitates (Fig. 5a and d) attributed to a strong chemical affinity of Al to Zr [32] and as Zr increases, the volume fraction of precipitates increases. It is also observed that, increase in addition of Zr above the solid solubility limit, i.e., greater than 0.1 wt% to the matrix, exhibited the presence of Cu_5Zr and $AlCu_2Zr$ phases. The Cu_5Zr corresponds to the uniform distribution of nanosized precipitates in the matrix [39–41], and $AlCu_2Zr$

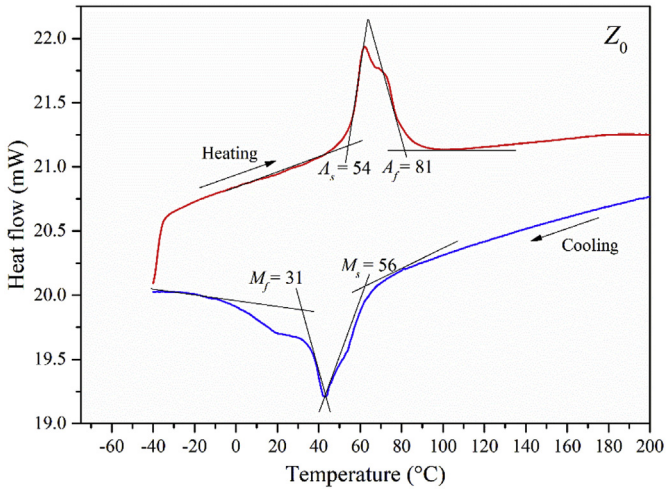

Fig. 6. Thermogram of alloy Z_0.

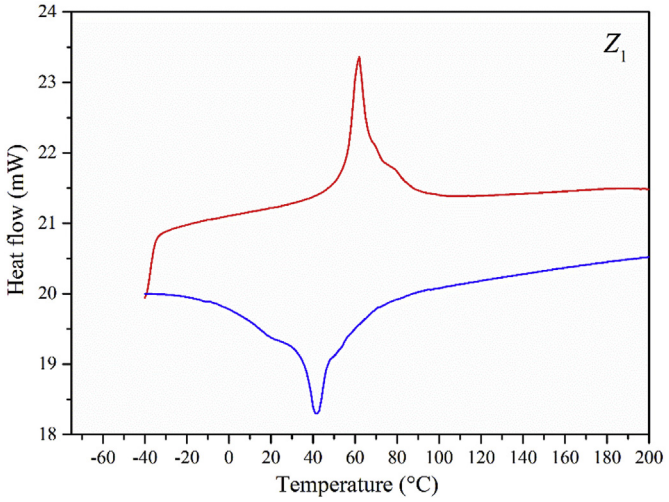

Fig. 7. Thermogram of alloy Z_1.

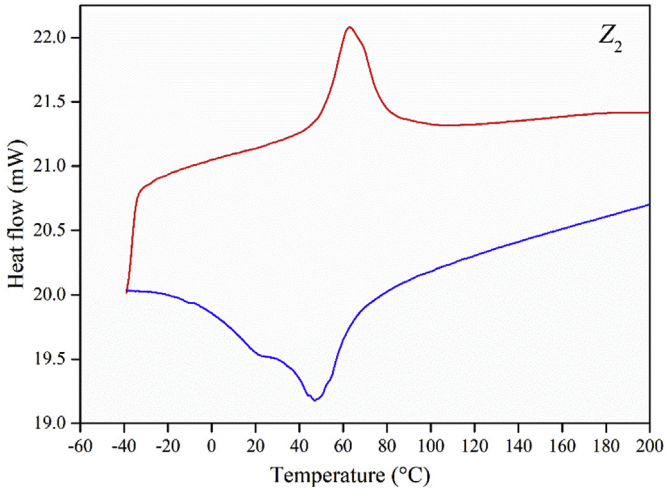

Fig. 8. Thermogram of alloy Z_2.

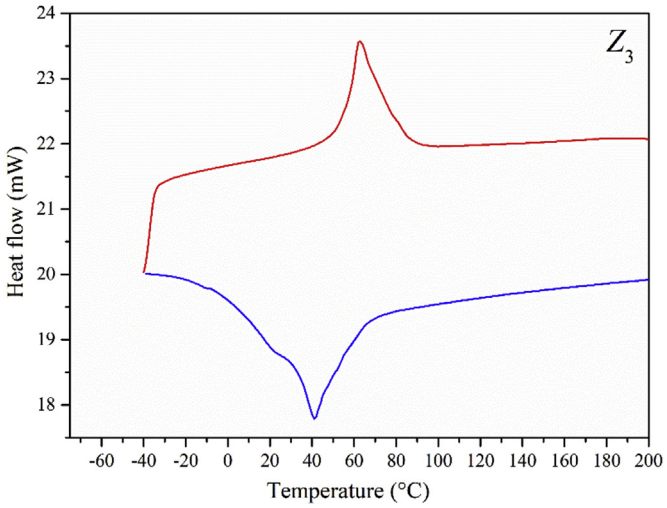

Fig. 9. Thermogram of alloy Z_3.

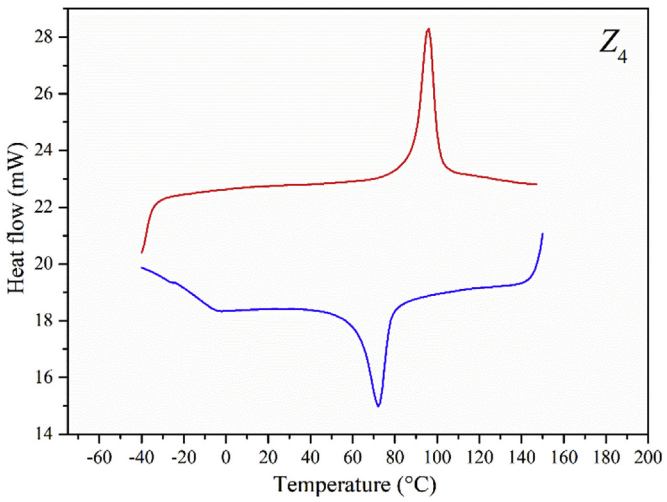

Fig. 10. Thermogram of alloy Z_4.

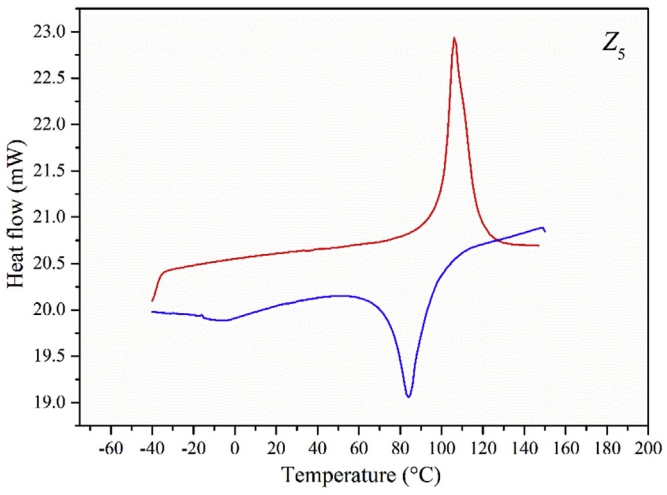

Fig. 11. Thermogram of alloy Z_5.

corresponds to the zirconium enriched precipitates at the grain boundaries (Fig. 3) are due to the diffusion of excess Zr towards grain boundaries [42] at elevated temperatures (betatization) and retained after quenching. The Z_4 and Z_5 exhibit the presence of ZrO2 (Fig. 5f and g) because the diffused Zr at the grain boundaries has a higher affinity towards O_2 [27] at elevated temperatures. The phases of β_1', γ_1', $ZrAl_3$, Cu_5Zr, Cu_2AlZr, and ZrO_2 were confirmed and indexed from ICDD 00-028-0005, 03-065-2750, 03-065-2250, 03-065-5906 and 03-065-2357

Table 1
Transformation temperatures (°C) and Enthalpies (J/g).

S. No	Alloy	M_f	M_s	$\Delta H_{A\rightarrow M}$	A_s	A_f	$\Delta H_{M\rightarrow A}$	Hysteresis ($A_f - M_s$)
1	Z_0	31	56	−14.8275	54	81	+9.7952	25
2	Z_1	32	50	−11.7067	55	68	+6.9593	18
3	Z_2	24	65	−14.3462	49	79	+7.8134	14
4	Z_3	25	54	−14.3391	56	78	+8.2263	24
5	Z_4	62	78	−6.5872	89	101	+6.5345	23
6	Z_5	73	92.5	−6.4610	101	115	+8.1282	23

Table 2
Mechanical properties of the alloys.

Alloy	Ultimate tensile strength (MPa)	Ductility (%)	Yield stress (0.2%) (MPa)	Yield strain (0.2%)
Z_0	363 ± 35	10.80 ± 0.75	132.34 ± 8.40	1.60 ± 0.03
Z_1	361 ± 15	13.20 ± 0.20	135.41 ± 22.61	1.71 ± 0.24
Z_2	545 ± 20	18.14 ± 0.29	114.48 ± 21.10	1.16 ± 0.35
Z_3	569 ± 05	21.90 ± 0.27	144.27 ± 5.79	1.62 ± 0.27
Z_4	667 ± 30	23.95 ± 0.86	147.03 ± 10.73	1.96 ± 0.15
Z_5	479 ± 13	10.59 ± 0.17	176.98 ± 13.23	1.70 ± 0.18

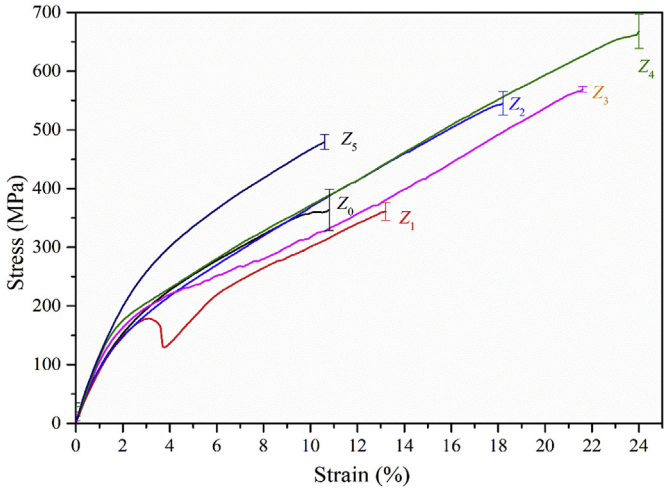

Fig. 12. Engineering tensile stress-strain curves of alloys; Z_0, Z_1, Z_2, Z_3, Z_4 and Z_5.

datasheets, respectively. Further, it is noticed that the prime diffraction peaks from the diffractograms as shown in Fig. 4 are (1 2 10) and (0 0 22) belonging to the martensite phase. The Intensity of the peak decreases with the broadening of width (Full Width Half Maximum) is an indicator of refinement in the crystallite size up to Z_4.

3.3. DSC curves

The thermoelastic martensitic transformation temperatures of the alloys were measured from the intersectional points of tangents at the base and sides of the thermograms as shown in Figs. 6–11, and are tabulated in Table 1. The curve with red color represents reverse transformation, i.e., from martensite to austenite, with the addition of heat (endothermic reaction) and curve with blue color represents forward transformation, i.e., austenite to martensite with the release of heat (exothermic reaction). It is perceived from Figs. 6–11 and Table 1, the addition of Zr didn't exhibit a rapid change in the transformation temperatures up to Z_2, and similar behavior is reported in Ref. [36]. Further, an addition of Zr shifts (inclined curves) towards higher temperatures [34] attributes to the distribution of fine second phase particles/intermetallics (precipitates), i.e., $ZrAl_3$, Cu_2AlZr, and Cu_5Zr in the matrix require an additional amount of energy for the phase transformation. It is also observed that the increase/decrease in Mf, Ms, enthalpies, and hysteresis are due to the size, vol. fraction and types of precipitates with variations in their elemental composition [43], leads to difficulties in design and developing an actuator for the requisite temperature.

3.4. Engineering tensile stress-strain curves and fractography

Addition of Zirconium refines the grains as shown in Fig. 3, and its influence on mechanical properties was measured by the unidirectional tensile tests. The measured engineering stress-strain data, i.e., ultimate tensile strength, ductility, yield stress (0.2% Proof stress) and yield strain of the alloys, are presented in Table 2 and also depicted in Fig. 12.

From the results, it is observed that Z_0 (Zr-free) has an ultimate tensile strength of 363 ± 35 MPa with ductility of 10.80 ± 0.75%, fails in cleavage mode as shown in Fig. 13a. The fracture surface of Z_0 shows that separation occurs along crystallographic planes, due to coarse grains (Fig. 3a) has low cohesive strength and high stress concentration at the grain boundaries [16]. As Zr increased to Z_1, i.e., 0.05 wt% to the matrix, it is observed an improvement in the ductility to 13.20 ± 0.20 with almost the same tensile strength of Z_0, i.e., 361 ± 15 MPa. The stress-strain curve of Z_1 exhibit a kink (Fig. 12) related to heterogeneous deformation, i.e., drop in the stress and then increases till fracture. Heterogeneous deformation attributed to distorted lattice arrangement and bimodal grains (variable sizes) as shown in Fig. 3b and c, and confirms from the mixed mode fracture surface as shown in Fig. 13b. Increase in Zr to Z_2, Z_3 and Z_4 exhibit a significant increase in tensile strengths, 545 ± 20, 569 ± 5and 667 ± 30 MPa with enhanced ductility of 18.14 ± 0.29, 21.90 ± 0.27 and 23.95 ± 0.86 respectively. The improvement in the properties are due to (a) finer the grain size, orientation of grains changes over small distances (Fig. 3d and e) increases in the length of the grain boundary, takes more deviations for the propagation of crack and requires more energy to move the dislocations [37]. (b) Formation and distribution of fine precipitates of $ZrAl_3$, Cu_5Zr [44,45] in the grains, prevents the movement of dislocations, subsequently increases the magnitude of critical stress for the deformation. It is worth to present, and highlight the factor affecting enhanced ductility of the alloys is Cu_5Zr phase, i.e., it has higher resistance to uniaxial deformation [45]. Increase in Zr increases the fine precipitates of Cu_5Zr in the alloy matrix, confirms from X-ray diffractogram (Fig. 4). The fractured surfaces as shown in (Fig. 13c – d), exhibit dimples (cavities) formed due to precipitates [29] and enlarged with the increase in loading till fracture confirms the ductile fracture. Further, the increase in Zr to Z_5 fails rapidly with the fall in tensile strength and ductility to 479 ± 13 MPa and 10.59 ± 0.17%, respectively as shown in Fig. 12. The failure attributes to hydrogen embrittlement (Fig. 13e and f), viz. insoluble Zr segregated at grain boundaries entraps oxygen into the lattice due to the high affinity at elevated temperature forms voids while quenching. However, the hydrogen molecule diffuses rapidly through the voids because of its small atomic radii and reacts with the entrapped oxygen forms water vapour. These vapour molecules exert higher pressure that is too large to diffuse out of the metal and splits the bonding between the grains, forming hydrides at the grain boundaries known as hydride cracking [46].

3.5. Shape memory test

The rolled and quenched alloy sheet at ≤ Mf temperature is completely twinned martensite as shown in Fig. 3, deforming (bending) at this stage undergoes martensite reorientation (detwinning) accompanied by their dislocation slip. Heating the deformed sheet above the austenite finish temperature tends to phase transformation i.e., from martensite to austenite by rearranging the variants, known as shape

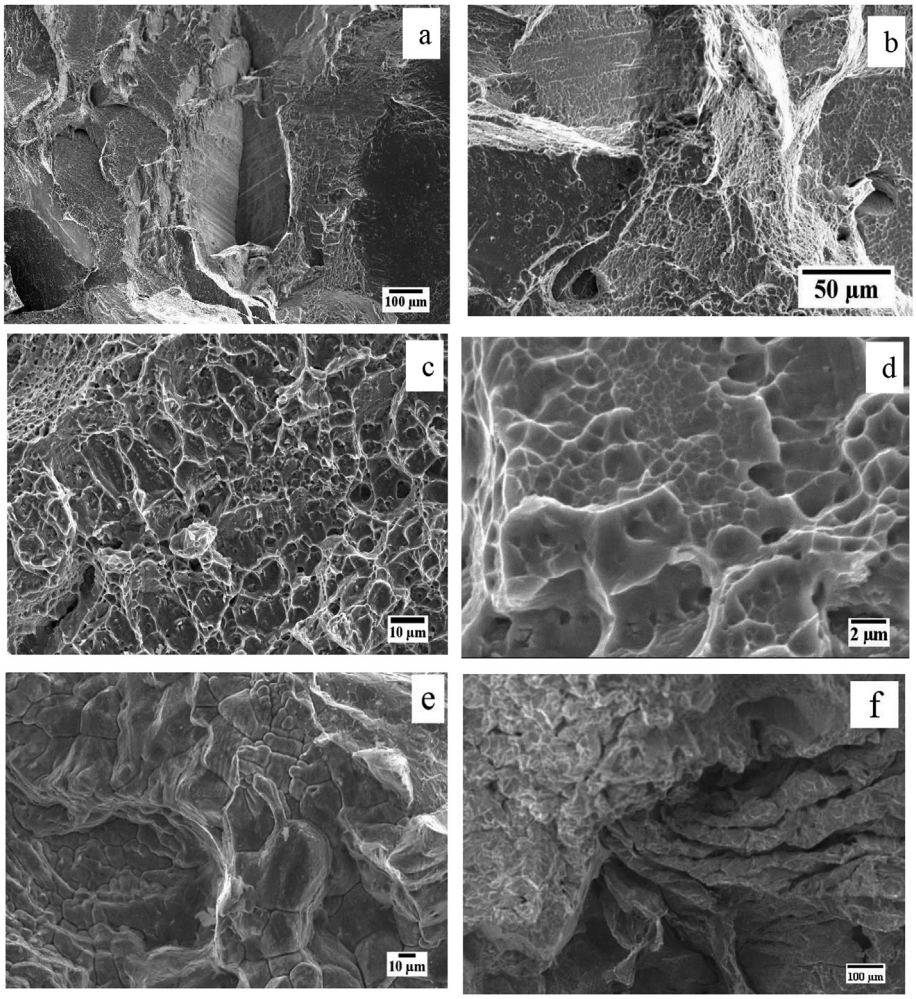

Fig. 13. Fracture surfaces of alloys; (a) Z_0, (b) Z_1, (c) Z_2, (d) Z_4, and (e) and (f) Z_5.

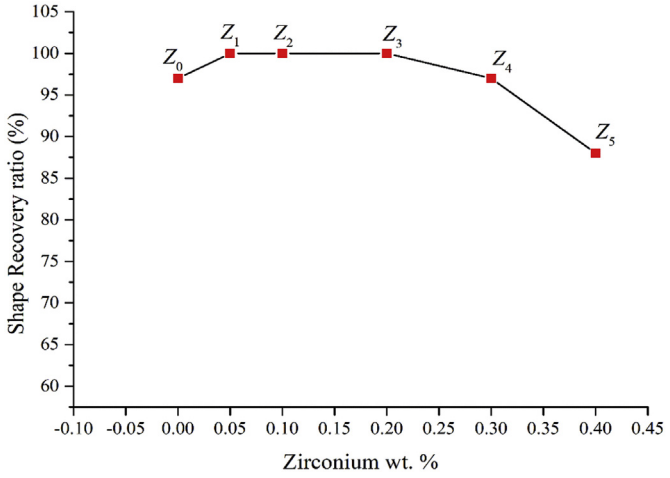

Fig. 14. Plot of shape recovery ratio *vs.* wt% of Zr.

memory effect. The potentiality of the prepared shape memory alloys was measured by the bend test as shown in Fig. 2. The shape recovery ratio of alloys was measured and the results are plotted in Fig. 14. From the results, it is observed that alloys Z_0 - Z_3, exhibit excellent shape recovery ratio of 100%, due to the larger grains has less grain boundary area which is easy to recover. The reduction in recovery was observed from Z_4 due to increasing Zr above solid solubility at room temperature forms:

i) various sizes of precipitates (Fig. 3) with increase/decrease in the elemental composition compared with the matrix alters the transformation temperatures entirely [47],
ii) rapid quenching from high temperatures (850 °C) creates more quenched-in vacancies in the fine grains leads to stabilization [48],
iii) finer the grains will possess different orientation of grains, and martensite variants which acts as a grain constraint and irregular grain boundaries create confusion path to revert back [49] and
iv) Precipitates at the grain boundary acts as a barrier for thermoelastic martensite plate movement, requires more energy to overcome the obstacles, supplying more energy tend to deteriorate the life of the actuator rapidly.

4. Conclusions

Effect of zirconium on the mechanical and shape memory properties of polycrystalline Cu-Al-Be shape memory alloy has been investigated by varying the Zr from 0.05 to 0.4 wt% with step 0.1 wt% to $Cu_{88.13}$-$Al_{11.42}$-$Be_{0.45}$ alloy. The conclusions drawn from the investigation are as follows:

- Zirconium acts as an effective grain refiner and reduces the grain size to 50.13 µm from 463.45 µm, i.e., 89.18% of reduction at 0.3 wt %, attributed to the low rate of grain growth exponent of Zr and heterogeneous nucleation.

- SEM studies presented the distribution of fine precipitates, i.e., $ZrAl_3$ and Cu_5Zr in the matrix and Zr enriched $CuAl_2Zr$ precipitates at the grain boundaries are ascribed to the low solid solubility of Zr in the matrix at room temperature.
- Increase in Zr increases of transformation temperatures due to the precipitates with varying elemental composition requires more heat energy for the phase transformation. Inconsistency in the transformation temperatures leads to difficulties in design and developing an actuator for the requisite temperature.
- Improvement in tensile strength to 667 ± 30 MPa and ductility 23.95 ± 0.86% at 0.3 wt% of Zr ascribed to precipitation strengthening. Insoluble Zr in the matrix agglomerates at the grain boundary causes hydrogen embrittlement failure.
- Alloys Z_1 to Z_3 exhibits excellent shape recovery ratio, i.e., 100% and deterioration in the ability from Z_4 to Z_5 are due to the pinning effect of precipitates at the grain boundaries.

Acknowledgement

The authors thank to Prof. S. Parida, Dept. of Metallurgical and Material Science, Indian Institute of Technology Bombay, India, for furnishing vacuum arc remelting machine to prepare Cu-Zr master alloys.

This study is financially supported by the SERB, Department of Science and Technology, Government of India, Project No: EMR/2016/001247.

References

[1] S. Barbarino, E.L. Saavedra Flores, R.M. Ajaj, I. Dayyani, M.I. Friswell, A review on shape memory alloys with applications to morphing aircraft, Smart Mater. Struct. 23 (2014), https://doi.org/10.1088/0964-1726/23/6/063001.
[2] S. Korkmaz, A review of active structural control: challenges for engineering informatics, Comput. Struct. 89 (2011) 2113–2132, https://doi.org/10.1016/j.compstruc.2011.07.010.
[3] L. Sun, W.M. Huang, Z. Ding, Y. Zhao, C.C. Wang, H. Purnawali, C. Tang, Stimulus-responsive shape memory materials: a review, Mater. Des. 33 (2012) 577–640, https://doi.org/10.1016/j.matdes.2011.04.065.
[4] D.C. Lagoudas, Shape Memory Alloys: Modeling and Engineering Applications, Springer Science & Business Media, 2008.
[5] J. Mohd Jani, M. Leary, A. Subic, M.A. Gibson, A review of shape memory alloy research, applications and opportunities, Mater. Des. 56 (2014) 1078–1113, https://doi.org/10.1016/j.matdes.2013.11.084.
[6] Z.G. WEI, R. Sandstroröm, S. MIYAZAKI, Shape memory materials and hybrid composites for smart systems Part II Shape-memory hybrid composites, J. Mater. Sci. 33 (1998) 3763–3783, https://doi.org/10.1023/100467463.
[7] C.A. Hsu, W.H. Wang, Y.F. Hsu, W.P. Rehbach, The refinement treatment of martensite in Cu–11.38wt.%Al–0.43wt.%Be shape memory alloys, J. Alloy. Comp. 474 (2009) 455–462, https://doi.org/10.1016/j.jallcom.2008.06.109.
[8] C. Aksu Canbay, A. Aydogdu, Thermal analysis of Cu-14.82 wt% Al-0.4 wt% Be shape memory alloy, J. Therm. Anal. Calorim. 113 (2013) 731–737, https://doi.org/10.1007/s10973-012-2792-6.
[9] S. Montecinos, A. Cuniberti, R. Romero, M. Stipcich, Grain size evolution in Cu-based shape memory alloys, J. Mater. Sci. 50 (2015) 3994–4002, https://doi.org/10.1007/s10853-015-8956-6.
[10] D. Dunne, K. Ireland, C. Gonzalez, M. Morin, G. Guenin, Hyperstabilisation of martensite in Cu-Al-Be alloys, Mater. Sci. Eng. 438–440 (2006) 339–342, https://doi.org/10.1016/j.msea.2006.02.139.
[11] I. Lopez-Ferreno, T. Breczewski, I. Ruiz-Larrea, A. Lopez-Echarri, M.L. No, J. San Juan, Thermal treatments and transformation behavior of Cu-Al-Be shape memory alloys, J. Alloy. Comp. 577 (2013) S463–S467, https://doi.org/10.1016/j.jallcom.2012.02.006.
[12] P. Zhang, A. Ma, J. Jiang, S. Lu, P. Lin, D. Yang, G. Liu, Microstructural evolution and mechanical response of Cu -Al - Be -B shape memory alloy processed by repetitive equal channel angular pressing, J. Alloy. Comp. 497 (2010) 210–214, https://doi.org/10.1016/j.jallcom.2010.03.014.
[13] S.N. Saud, E. Hamzah, T. Abubakar, M.K. Ibrahim, A. Bahador, Effect of a fourth alloying element on the microstructure and mechanical properties of Cu – Al – Ni shape memory alloys, J. Mater. Res. 30 (2015) 2258–2269, https://doi.org/10.1557/jmr.2015.196.
[14] C.A. Canbay, V. Sampath, Microstructural and thermal investigations of Cu-Al-Mn-Ni shape memory alloys microstructural and thermal investigations of Cu-Al-Mn-Ni, mater. Today Proc 4 (2017) 10682–10689, https://doi.org/10.1016/j.matpr.2017.08.014.
[15] T.A.A. Melo, D.F. De Oliveira, S.J.G. Lima, V.T.L. Buono, R.M. Gomes, Nb modifified Cu-AI-Be shape memory alloys, Int. Conf. Martensitic Transform, John Wiley & Sons, Inc., 2009, pp. 591–594.
[16] G.V.D.M. Candido, T.A.D.A. Melo, V.H.C. De Albuquerque, R.M. Gomes, S.J.G. De Lima, J.M.R.S. Tavares, Characterization of a CuAlBe alloy with different Cr contents, J. Mater. Eng. Perform. 21 (2012) 2398–2406, https://doi.org/10.1007/s11665-012-0159-6.
[17] R. Dasgupta, A.K. Jain, P. Kumar, S. Hussain, A. Pandey, Role of alloying additions on the properties of Cu – Al – Mn shape memory alloys, J. Alloy. Comp. 620 (2015) 60–66, https://doi.org/10.1016/j.jallcom.2014.09.047.
[18] U.S. Mallik, V. Sampath, Effect of alloying on microstructure and shape memory characteristics of Cu-Al-Mn shape memory alloys, Mater. Sci. Eng. 481–482 (2008) 680–683, https://doi.org/10.1016/j.msea.2006.10.212.
[19] S. Ergen, O. Uzun, F. Yilmaz, M.F. Kiliçaslan, Shape memory properties and microstructural evolution of rapidly solidified CuAlBe alloys, Mater. Char. 80 (2013) 92–97, https://doi.org/10.1016/j.matchar.2013.03.010.
[20] E.M. Mazzer, C.S. Kiminami, P. Gargarella, R.D. Cava, L.A. Basilio, C. Bolfarini, W.J. Botta, J. Eckert, T. Gustmann, S. Pauly, Atomization and selective laser melting of a Cu-Al-Ni-Mn shape memory alloy, Mater. Sci. Forum 802 (2014) 343–348 https://doi.org/10.4028/www.scientific>.net/MSF.802.343.
[21] M. Izadinia, K. Dehghani, Structure and properties of nanostructured Cu-13.2Al-5.1Ni shape memory alloy produced by melt spinning, Trans. Nonferrous Metals Soc. China 21 (2011) 2037–2043, https://doi.org/10.1016/S1003-6326(11)60969-2.
[22] A. Ostovari, M. Arash, M. Mostafa, Effect of accumulative roll bonding and equal channel angular rolling on microstructural and mechanical properties of Cu – Al – Mn shape memory alloys, Trans. Indian Inst. Met. 70 (2017) 1901–1909, https://doi.org/10.1007/s12666-016-1007-4.
[23] S.N. Saud, E. Hamzah, T. Abubakar, S. Farahany, Structure-property relationship of Cu-Al-Ni-Fe shape memory alloys in different quenching media, J. Mater. Eng. Perform. 23 (2014) 255–261, https://doi.org/10.1007/s11665-013-0759-9.
[24] V. Sampath, Effect of Thermal Processing on Microstructure and Shape-Memory Characteristics of a Copper – Zinc – Aluminum Shape-Memory Alloy Effect of Thermal Processing on Microstructure and Shape-Memory Characteristics of a Copper – Zinc – Aluminum Shape-Memory All, (2007), pp. 37–41, https://doi.org/10.1080/10407780601015808.
[25] P. Zhang, A. Ma, S. Lu, P. Lin, J. Jiang, H. Ma, C. Chu, Effect of equal channel angular pressing and heat treatment on the microstructure of Cu-Al-Be-B shape memory alloy, Mater. Lett. 63 (2009) 2676–2679, https://doi.org/10.1016/j.matlet.2009.09.037.
[26] F.J. Gil, J. Pena, J.M. Guillemany, Improvement of the grain refinement of Cu-Zn-Al shape memory alloys with manganese , cobalt , and zirconium addition, J. Mater. Synth. Process. 7 (1999) 127–133.
[27] S. Matsuoka, M. Hasebe, R. Oshima, F.E. Fujita, Improvement of ductility of melt spun Cu – Al – Ni shape memory alloy ribbons by addition of Ti or Zr, Jpn. J. Appl. Phys. 22 (1983) 528–530.
[28] J.S. Lee, C.M. Wayman, Grain refinement of a Cu–Al–Ni shape memory alloy by Ti and Zr additions, Trans. Inst. Jpn. Met. 27 (1986) 584–591.
[29] J.S. Lee, C.M. Wayman, Grain refinement of Cu-Zn-AI shape memory alloys, Metallography 19 (1986) 401–419.
[30] J.W. Kim, D.W. Roh, E.S. Lee, Y.G. Kim, Effects on microstructure and tensile properties of a zirconium addition to a Cu-AI-Ni shape memory alloy, Metall. Trans. A. 21A (1990) 741–744.
[31] D.W. Roh, J.W. Kim, T.J. Cho, Y.G. Kim, Tensile properties and microstructure of microalloyed Cu-Al-Ni-X shape memory alloys, Mater. Sci. Eng. A136 (1991) 17–23.
[32] S. Bhattacharya, A. Bhuniya, M.K. Banerjee, Influence of minor additions on characteristics of Cu-AI-Ni alloy, Mater. Sci. Technol. 9 (1993) 654–658.
[33] C. Hsu, W. Wang, Superplastic forming characteristics of a Cu-Zn-A1-Zr memory alloy, 205 (1996) 247–253.
[34] V. Sampath, Studies on the effect of grain refinement and thermal processing on shape memory characteristics of Cu–Al–Ni alloys, Smart Mater. Struct. 14 (2005) S253–S260, https://doi.org/10.1088/0964-1726/14/5/013.
[35] V. Sampath, Improvement of shape-memory characteristics and mechanical properties of copper – zinc – aluminum shape- memory alloy with low aluminum content by grain refinement improvement of shape-memory characteristics and mechanical properties of copper – zinc – Al, Mater. Manuf. Procesees. 21 (2006) 789–795, https://doi.org/10.1080/10426910600837756.
[36] V. Sampath, U.S. Mallik, Influence of minor additions of boron and zirconium on shape memory properties and grain refinement of a Cu-Al-Mn shape memory alloy, ESOMAT 2009 - 8th Eur. Symp. Martensitic Transform, 200905028, , , https://doi.org/10.1051/esomat/200905028.
[37] J. Yang, Q.Z. Wang, F.X. Yin, C.X. Cui, P.G. Ji, B. Li, Effects of grain refinement on the structure and properties of a CuAlMn shape memory alloy, Mater. Sci. Eng. 664 (2016) 215–220, https://doi.org/10.1016/j.msea.2016.04.009.
[38] J.R. Davis, A.S.M.I.H. Committee, Copper and Copper Alloys, ASM International, 2001, https://books.google.co.in/books?id=sxkPJzmkhnUC.
[39] L.M. Bi, P. Liu, X.H. Chen, X.K. Liu, W. Li, F.C. Ma, Analysis of phase in Cu-15%Cr-0.24%Zr alloy, Trans. Nonferrous Met. Soc. China (English Ed. 23 (2013) 1342–1348, https://doi.org/10.1016/S1003-6326(13)62602-3.
[40] Z.Y. Pan, J.B. Chen, J.F. Li, Microstructure and properties of rare earth-containing Cu-Cr-Zr alloy, Trans. Nonferrous Met. Soc. China (English Ed. 25 (2015) 1206–1214, https://doi.org/10.1016/S1003-6326(15)63717-7.
[41] L.J. Peng, X.J. Mi, B.Q. Xiong, H.F. Xie, G.J. Huang, Microstructure of phases in a Cu–Zr alloy, Rare Met. 34 (2015) 706–709, https://doi.org/10.1007/s12598-014-0324-1.
[42] T. Gustmann, J.M. dos Santos, P. Gargarella, U. Kühn, J. Van Humbeeck, S. Pauly, Properties of Cu-based shape-memory alloys prepared by selective laser melting, Shape Mem. Superelasticity. 3 (2017) 24–36, https://doi.org/10.1007/s40830-016-0088-6.

[43] H. Flores Zuniga, S. Belkahla, G. Guénin, The thermal aging and two way memory effect (TWME) IN Cu-Al-Be shape memory alloy, J. Phys. III 1 (1991) 289–294.
[44] Y. Ye, X. Yang, J. Wang, X. Zhang, Z. Zhang, T. Sakai, Enhanced strength and electrical conductivity of Cu-Zr-B alloy by double deformation-aging process, J. Alloy. Comp. 615 (2014) 249–254, https://doi.org/10.1016/j.jallcom.2014.07.010.
[45] G. Yi, X. Zhang, J. Qin, J. Ning, S. Zhang, M. Ma, R. Liu, Mechanical , electronic and thermal properties of Cu 5 Zr and Cu 5 Hf by first-principles calculations, J. Alloy. Comp. 640 (2015) 455–461.
[46] M.M. Schwartz, Brazing, second ed., ASM International, 2003.
[47] K. Otsuka, C.M. Wayman, Shape Memory Materials, Cambridge University Press, 1999, https://books.google.co.in/books?id=DvItE9XUlN8C.
[48] M. Chandrasekaran, E. Cesari, J. Wolska, I. Hurtado, R. Stalmans, J. Dutkiewicz, Stabilisation of martensite in copper based shape memory alloys, J. Phys. IV 5 (1995) 143–152.
[49] G.N. Sure, L.C. Brown, The mechanical properties of grain refined beta-cuaini strain-memory alloys, Metallurg 15 (1984) 1613–1621.